Characterizing assembly morphology changes during solubilization process of dimyristoyl phosphocholine vesicles by *n*-dodecyl triethylammonium bromide

Shaoqing Wang [a], Jianbin Huang [a,*], Qian Song [a], Honglan Fu [b]

[a] *State Key Laboratory for Structural Chemistry of Unstable and Stable Species, College of Chemistry and Molecular Engineering, Peking University, Beijing 100871, People's Republic of China*
[b] *College of Life Science, Peking University, Beijing 100871, People's Republic of China*

Abstract

In the present work, the assembly morphology changes during the solubilization process of the sonicated unilamellar vesicles from dimyristoyl phosphocholine (DMPC) by a cationic surfactant, *n*-dodecyl triethylammonium bromide (DTEAB) were well characterized with DSC, FF-TEM and DLS and fluorescence probes technique. Based on an analysis on the above results, a primary multi-stage model was brought forward to sketch the assembly morphology changes during the DMPC vesicle solubilization by DTEAB. In comparison with classical models, vesicles division, tubule-like structure formation and fission to vesicle were found in the middle stages of this model. Additionally, it is the first time that the transversally-cut profiles of tubule-like structures were observed during vesicle solubilization process.
© 2007 Elsevier Inc. All rights reserved.

Keywords: Tubule-like; Vesicle solubilization; Vesicle enlargement; Vesicle fusion; Vesicle (tubule) fission

1. Introduction

From the finding of similarity between lipid vesicles and cells, the previous studies on cell solubilization had turned to study lipid vesicles solubilization [1], especially on the morphology transformation mechanism of assemblies in this process [2–4]. Therefore, three-stage model [3] was proposed in the 1980's. In the first stage of this model, first surfactant molecules participate into lipid vesicles membrane up to a critical saturated concentration. Beyond this concentration, the system enters into the second stage, where lipid-saturated mixed micelles form and coexist with the mixed vesicles together until all the vesicles have been solubilized. Then the third stage began, during which the vesicle solubilization has completed and only mixed micelles exist in system. In fact, the assembly morphology changes during vesicles solubilization [5] are more complicated than that described in the above model, for example, the complicate pattern of turbidity changes found in Inoue et al.'s study on DLPA vesicles solubilization by TTABr [6], the lamellar structures, perforated vesicles, disc-like lamellar sheets and the micelle-network observed in solubilization of lecithin vesicles with other surfactant [7,8] as well as the tubule-like structures observed from transversally-cut profile during the process characterized in the present work.

Hence, the molecular mechanism of assembly morphology changes during vesicle solubilization is not yet fully elucidated from a physicochemical point of view. Further efforts were needed to disclose the underline rules as done by Edwards and Almgren [2], etc. For a comprehensive understanding of the above assembly transformation, a detail examination on the general morphology feature of these assemblies is necessary in addition to the special inspection of TEM, DLS and SANS, etc. In pursuing the information about the structure and dynamics of assemblies, fluorescence probe technique is favorable with consideration of their little disturbance on original assembly structure [9,10]. 1,6-Diphenyl-1,3,5-hexatriene (DPH) [11,12] and pyrene [10] are the most frequently used fluorescence probe

for this purpose. Usually, DPH fluorescence anisotropy indicates the common fluidity of membrane [13], I_1/I_3 value of pyrene [10] fluorescence is correlated to the membrane polarity of assemblies in system. Therefore, a combined analysis on the variation of DPH anisotropy and pyrene I_1/I_3, can provide preliminary information about the morphology behavior of assemblies in one sequential process, such as the nature fluctuation of different positions in membrane.

Thermodynamically, the assembly morphology changes must result to the variation of energy needed for chain isomerism or lateral expansion during the gel-to-liquid crystalline phase transition. Therefore, the excursion and appearance of new gel-to-liquid crystalline phase transition temperature (T_m) on DSC curves can also be used to monitor the composition or structural difference of present assemblies [14,15] in system. Additionally, DLS measurements and TEM observation can provide a relative size distribution and direct morphology observation of assemblies during the example process, respectively.

In the present work, a primary multi-stage model divided by five transition steps was proposed to describe the assembly morphology changes during DMPC vesicle solubilization by a cationic surfactant, DTEAB based on the analysis on all the data obtained by above techniques. Being different from the classical three-stage model, the middle transition steps of this proposed model include vesicles division, tubule-like structure formation and fission to vesicle again etc, not one slow transition process from mixed-vesicles to mixed-micelles alone. Additionally, it is the first time that the transversally-cut profiles of tubule-like structures were observed during vesicle solubilization process.

2. Materials and methods

1,2-Ditetradecanoyl-*sn*-glycero-3-phosphocholine (purity 99%) was obtained from Sigma and used without further purification. 1,6-Diphenyl-1,3,5-hexatriene (DPH) (Purity 98%) was from ACROS ORGANICS Co. (USA). *n*-Dodecyl triethylammonium bromide (DTEAB) was prepared by reaction of bromododecane and triethylamine and the product purity was examined by NMR and elemental analysis. The cmc of DTEAB is 1.3×10^{-2} mol/l according to its surface tension curve determined by drop volume method. Redistilled water from potassium permanganate solution was used in all the experiments. The other reagents were all of A.R. Grade and used without purification. In this work, all the experiment was performed at 30 °C when no special indication.

2.1. Preparation of unilamellar vesicles from DMPC

In a pear-shaped flask, 20 mg DMPC was well dissolved in 5 ml chloroform and then the solvent was removed by a rotary evaporator. After blowing out the remnant solvent with gaseous nitrogen, the flask was kept in a vacuum desiccator filled with nitrogen for overnight. Then the dried DMPC film on the inside wall of the flask was hydrated with 5 ml of water. The formed multilamellar vesicles suspension was sonicated using

a Ultrasonicator JY92-II (SCIENTZ, Ningbo, China) equipped with a titanium microprobe in a water cup (30 °C) connected with a thermostat cooling bath (Mgw Lauda RM6, KRUSS, Germany) for absorbance of the heat produced during sonication. The dispersion was sonicated until no further change in turbidity, which was measured at 500 nm using a UV–visible spectrophotometer (Cary 1E, Varian Australia PTY Ltd.). Centrifugation (12000 rpm, 30 min) was performed to remove the titanium powder falling during sonication.

2.2. DPH fluorescence anisotropy and pyrene I_1/I_3 determination

To the prepared 1 ml of individual or mixed sample of DMPC vesicle suspension/DTEAB solution, 10 μl of fluorescence probe solution (DPH, 1×10^{-4} mol/l; pyrene, 1×10^{-5} mol/l) was added, which was diluted from the stored solution (1×10^{-3} mol/l of DPH or pyrene in THF) with redistilled water. Probe containing samples were maintained overnight at 30 °C in a dark chamber of water bath. The fluorescence measurement was performed with an F-4500 spectrofluorometer (Hitachi, Japan). Briefly, 0.5 ml of sample was added into a small cuvette of quartz glass with 5 mm light pathlength in both directions. During fluorescence measurement, the temperature of samples was maintained at the same temperature (30 °C) with a circulating water bath. The wavelength bandwidth was set ±5 nm. And 5 nm of slit width was set for both the excitation and emission beams during measurement. DPH was excited at 357 nm and its emitted fluorescence intensity was recorded at 433 nm. Pyrene was excited at 333 nm and its emitted fluorescence intensity at 374 and 386 nm was recorded as I_1 and I_3, respectively. For all fluorescence emission measurements in this work, the effect caused by light scattering of a blank sample was less than 1%. The steady-state DPH fluorescence anisotropy (r) was calculated according to [11]:

$$r = \frac{I_{||} - GI_{\perp}}{I_{||} + 2GI_{\perp}}. \tag{1}$$

Here, $I_{||}$ and $I_{\perp}$ are the fluorescence intensity detected through a polarizer oriented parallel and perpendicular to the vertical-polarization phase of the excitation light beam, respectively, and $G = (i_{||}/i_{\perp})$ is a sensitivity factor of the machine detection for vertically and horizontally polarized light. $i_{||}$ and $i_{\perp}$ are, respectively, the fluorescence intensity detected through a polarizer oriented parallel and perpendicular to the horizontal-polarized excitation light.

2.3. Dynamic light scattering (DLS) measurement

Dynamic light scattering measurements were performed with a spectrometer (ALV-5000/E/WIN Multiple Tau Digital Correlator) and a Spectra-Physics 2017 200 mW Ar laser (514.5 nm wavelength). The scattering angle was 90°. The distribution of hydrodynamic radius R_h was deduced by analyzing the intensity autocorrelation functions using the Contin method. The system apparent hydrodynamic radius $\langle R_h \rangle$ was deduced from the intensity autocorrelation functions being analyzed using the Cumulant method.

2.4. Differential scanning calorimetry (DSC)

Thermotropic phase transition parameters of all samples were measured on a Q100 ultrasensitive scanning calorimeter (TA, America), which has a sensitivity of 0.2 μW. Aluminum pans were hermetically sealed and used as the sample container. Heating–cooling cycles were scanned between 0 and 60 °C at a rate of 2 °C/min.

2.5. Freezing-fracture transmission electron microscopy (FF-TEM)

Replica for TEM observation was prepared by freeze-fracture method. In detail, sample was frozen in liquid nitrogen until liquid surface became calm. Then the sample was fractured in a JEE-4X etching system at the vacuum less than 1.33×10^{-3} Pa and etched for 1 min by heating to $-100 - -110$ °C. The fracture surface was immediately replicated by spraying a platinum carbon mixture from an electrode at a 45 °C angle and a thick film of carbon at normal incidence to the fracture surface of the replica. The replicas were collected on formvar-coated 230 mesh copper electron microscope grids and observed on a JEM-100 CX(II) transmission electron microscope in the conventional transmission mode using 80-kV electrons.

3. Results

3.1. DPH fluorescence anisotropy r and I_1/I_3 of pyrene fluorescence

Fluorescence anisotropy r of DPH and I_1/I_3 of pyrene were, respectively, showed as the function of the logarithmic DTEAB concentration in Fig. 1. On the r curve, one peak was observed at 8 mmol/l DTEAB. At low concentration of DTEAB, r first declined rapidly from 0.14 for pure DMPC vesicle to a short plateau at 0.10 level, and then decreased slowly to 0.08. After passing the peak ($r = 0.120$), r decreased again and finally reached 0.05 for 16 mmol/l DTEAB, same as in pure DTEAB micelles system (20 mmol/l). In the case of pyrene probe, I_1/I_3 decreased a little from 1.10 for pure DMPC vesicle to 1.08 at low concentration of DTEAB before a continual slow increasing until 1.14 at 6 mmol/l DTEAB. With further addition of DTEAB, the I_1/I_3 curve deflected to fast increasing until 1.45 of pure DTEAB micelle system (20 mmol/l). Similar changing pattern for I_1/I_3 of pyrene was also observed in the Inoue's work about the solubilization of DPPC vesicles by $C_{10}E_7$ [16].

3.2. Differential scanning calorimetry (DSC)

The DSC curves were collected in Fig. 2. At first, the gel–liquid crystal phase transition temperature T_m of vesicles decreased with the addition of DTEAB into system, e.g. from 24 °C (T_m of pure DMPC vesicles) to 21.5 °C when DTEAB concentration increased from 0 to 0.2 mmol/l. Interestingly, a new phase appeared with high T_m at 45.2 and 40.5 °C in addition to the phase of low T_m at 13 and 8.9 °C for samples
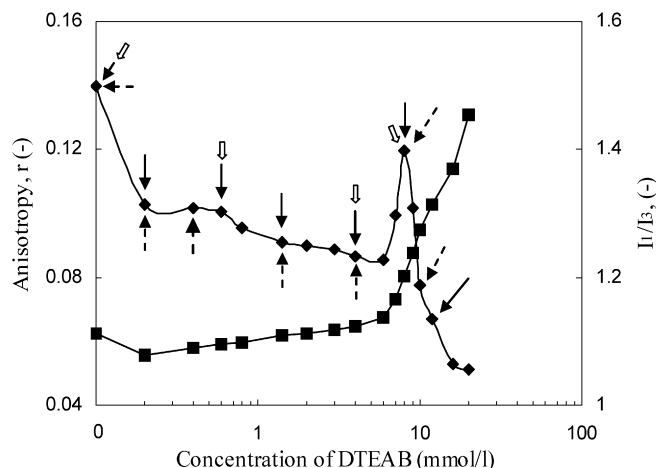
Fig. 1. Fluorescence anisotropy r of DPH (♦) and I_1/I_3 of pyrene (■) for DMPC vesicles mixed with different concentration of DTEAB. In the figure, the beginning and end points represent the pure DMPC vesicles (2 mmol/l of DMPC) and DTEAB solution (20 mmol/l of DTEAB), respectively. In all the other samples, DMPC concentration was constant 2 mmol/l, but DTEAB concentration is different. The shown data were the average of triplicate experiments. In the figure, the empty arrows, the real line and dashed line arrows indicate the selected samples for FF-TEM, DSC and DLS inspection, respectively.
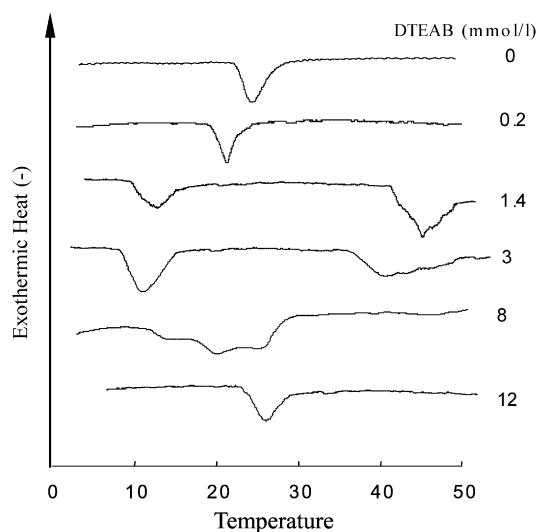
Fig. 2. DSC curves of DMPC vesicles/DTEAB mixture for which 2 mmol/l DMPC vesicles were mixed with different concentration of DTEAB.

containing 1.4 and 3.0 mmol/l DTEAB, respectively. On the curve of 8 mmol/l DTEAB, both exothermic enthalpy peaks of low and high T_m disappeared, and were replaced by two overlapped peaks, centering at 20.3 and 25.5 °C, respectively. When more DTEAB was added, e.g. sample containing 12 mmol/l, only one peak was observed again at 26.3 °C, which may be the peak of micellization and demicellization process as observed in Majhi and Blume's work [17].

3.3. Freeze-fracture TEM

The assembly pictures of freeze-fracture transmission electron microscope specimens were showed in Fig. 3. These spec-
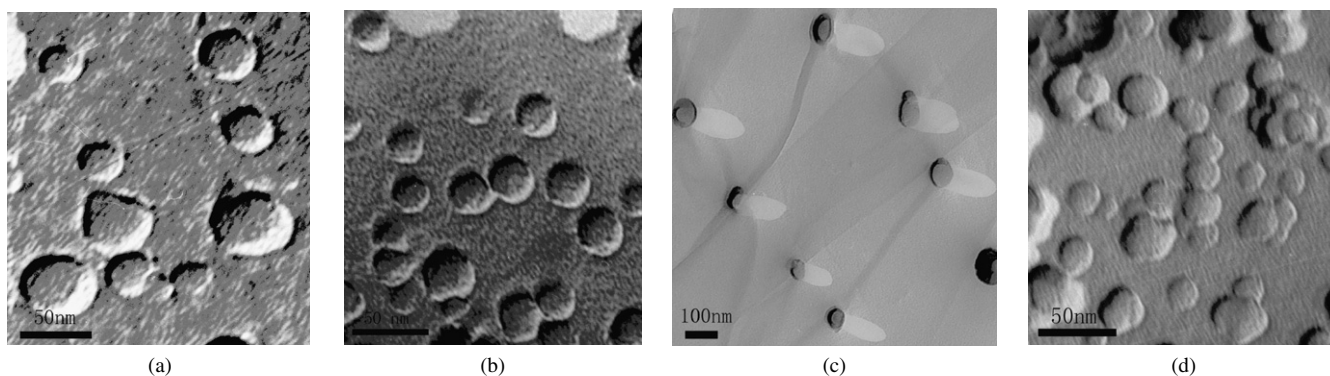
Fig. 3. Freeze-fracture TEM of DMPC vesicle/DTEAB mixture. DMPC concentration was constant, 2 mmol/l. DTEAB concentration was, respectively, (a) 0, (b) 0.6, (c) 3 and (d) 8 mmol/l.
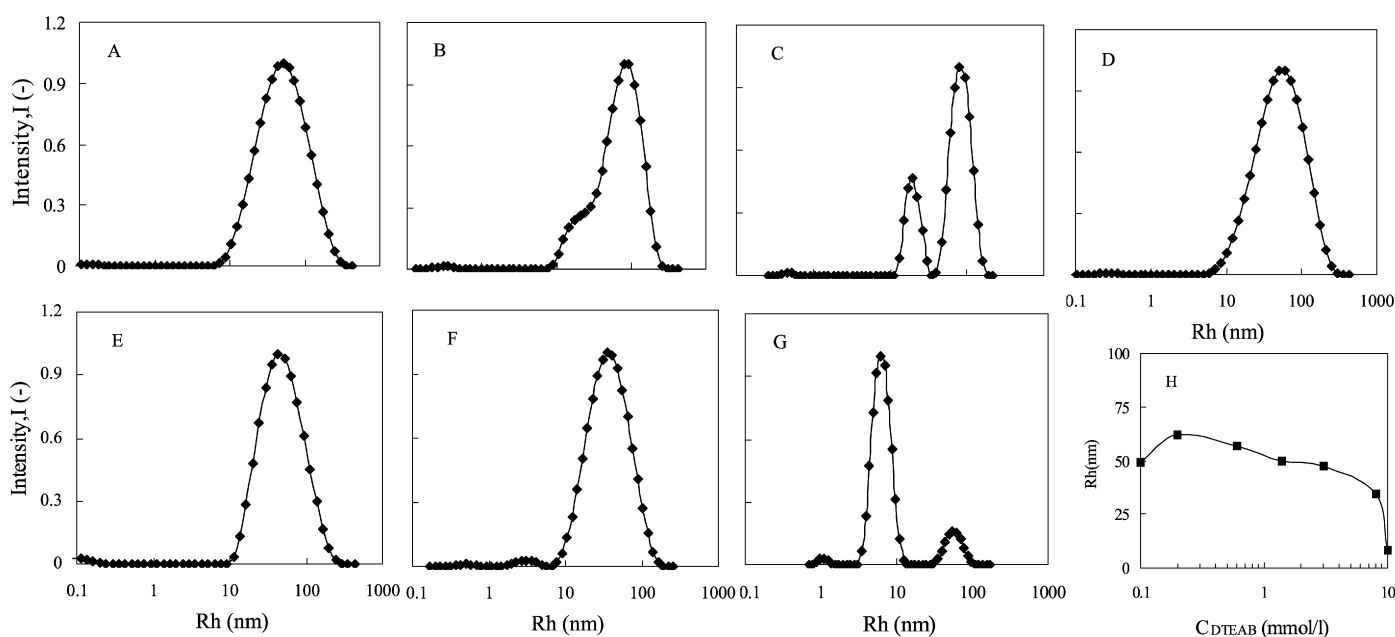
Fig. 4. (A)–(G) Distribution of hydrodynamic radius R_h for DMPC vesicle/DTEAB mixture determined by dynamic light scattering measurement (Contin correlation). DMPC concentration was constant, 2 mmol/l. DTEAB concentration was (A) 0, (B) 0.2, (C) 0.4, (D) 1.4, (E) 3, (F) 8 and (G) 10 mmol/l; (H) average dynamic radius $\langle R_h \rangle$ of all the samples as a function of the containing DTEAB concentration (Cumulant correlation).

imens were selected according to fluorescence results (Fig. 1). Pure DMPC vesicles were observed with 25–50 nm in diameter (Fig. 3a). After being mixed with 0.6 mmol/l DTEAB, a little smaller but more uniform vesicles were seen in Fig. 3b. When more DTEAB was mixed in this system, e.g., 3 mmol/l, some cross-sectioned tubule-like assemblies were found in Fig. 3c. In principle, the shadow of vesicles (convex or concave) resembles one third or less of one ellipse in shape. But the shadow of the new structure in Fig. 3c exhibits a shadow of two third or more of one ellipse in shape. Therefore, this new assemblies observed in TEM (Fig. 3c) were considered as tubules-like structure protruding out of the fracture surface of specimens according to the etching effect. In the case of 8 mmol/l DTEAB, vesicles were found again as shown in Fig. 3d. With higher concentration of DTEAB, micelles formed no vesicles were observed.

3.4. Dynamic light scattering (DLS)

The hydrodynamic radius R_h distribution for the selected samples were shown in Figs. 4A–4G as a function of DTEAB concentration when the data were analyzed with Contin correlation function. In Fig. 4H showed the changing tendency of hydrodynamic radius $\langle R_h \rangle$ with increasing DTEAB concentration when the data were analyzed with Cumulant correlation. At first, $\langle R_h \rangle$ increased to a maximal value when DTEAB concentration increased to 0.2 mmol/l, at which the system showed a deflective sinusoidal mode in Fig. 4B. In the following, a clear bimodal distribution of Rh was observed in Fig. 4C, which might indicate vesicles fission following the initial vesicle enlargement stage. Simultaneously, $\langle R_h \rangle$ deflected to decrease slowly until 35 nm with the further addition of DTEAB up to 8 mmol/l. At 10 mmol/l of DTEAB, $\langle R_h \rangle$ decreased sharply to a value about 8 nm. This agreed well with R_h distribution

showed in Fig. 4G, where a big peak was observed centering at several nanometers. This suggested that a large amount of micelles had formed following the vesicles solubilization. As for the sample of Fig. 4E, a obviously higher value was obtained for assembly size when both DMPC vesicle suspension and DTEAB solution was filtered off dust before mixing (Fig. S1 in supplementary material). This indicated that the size examination of the present tubule-like assemblies was probably affected by the filter process before DLS examination.

4. Discussion

In this work, fluorescence probe technique (DPH anisotropy and pyrene I_1/I_3) provided important information to sample selection for DSC, TEM and DLS etc. inspection on the phase and morphology changes of assemblies during the vesicle solubilization process. Consequently, a combined data analysis gave a description for the morphology change process of assemblies during DMPC vesicles solubilization by DTEAB. In the following, the whole model solubilization process was divided into five transition steps and a brief outline of this multi-stage model was presented.

4.1. Vesicle enlargement

Vesicle enlargement in the initial of vesicle solubilization was observed according to DLS examination. In Fig. 4H, $\langle R_h \rangle$ increased from 49 nm of original DMPC vesicles to 64 nm with the addition of DTEAB to 0.2 mmol/l. In literature, vesicle size growth has been often detected with phosphatidylcholine (PC) vesicles at low concentration of surfactants [7,21,22]. The reason was explained as the swelling effect of the added surfactant on PC vesicles [22]. Additionally, the insertion of DTEAB molecules into lipid bilayer resulted in a higher fluidity of the membrane interior (where DPH molecules were buried [11, 12]), and in palisade layer (where pyrene molecules stayed [10,18]) as shown by the decrease of r and I_1/I_3 in Fig. 1. Meanwhile, the mixed vesicle bilayer displayed a lower phase transition temperature T_m (21.5 °C at 0.2 mmol/l DETAB) than that for pure DMPC vesicles (24 °C) (Fig. 2). The accompanied T_m decrease was also observed in the mixture of DPPC vesicles with sodium (deoxy)cholate in water [19], and DMPC vesicles with $C_{10}E_6$ [20]. This indicates that the added surfactant molecules disturbed the packing order of lipid in the bilayer membrane of vesicles.

4.2. Vesicles fission

When DTEAB content passes a threshold concentration, the increased lateral tension inside vesicle membrane limits the further enlargement of vesicles. On the other hand, the addition of DTEAB may induce asymmetric distribution in lipid bilayer as well as the phase separation and positive spontaneous curvature towards the exterior of the bilayer [24]. Budding and fission of liquid-ordered microdomain to form vesicles from big unilamellar vesicles had been observed with phase-contrast and fluorescence microscope during the interaction of detergents,

Lyso-PC, Triton X-100 and Brij98 with mixed PC vesicles [25,26].

Here, the vesicle fission was shown clearly from the bimodal distribution of R_h in Fig. 4C, before which the system showed a largely-deflective sinusoidal mode of R_h distribution (Fig. 4B). Some information about the fission can also be obtained from the fluorescence results. The increased bilayer curvature of vesicles hardly affected the interior nature of membrane where DPH molecules presented [23], but brought a little impact on the palisade layers as shown by the slowly increasing I_1/I_3 of pyrene [10,16] (Fig. 1). Fig. 3b showed that the predominating assemblies were still vesicles at 0.6 mmol/l DTEAB, but no obvious vesicle size changes are observable in TEM picture. However, the vesicles shape and size were more uniform than the original DMPC vesicles in Fig. 3a. This may indicate that the spontaneous vesicle fission occurred in the system and the newly-produced small vesicles from the fission increased in diameter because of the incorporation of more DTEAB molecules. Both the above fission and the following fusion of vesicles as well as the final tubules fission, are a result of minimizing the energy function with contributions arising from bending resistance, lateral tensions, line tension and normal pressure difference [27].

4.3. Tubules formation

When DTEAB concentration was higher than 0.6 mmol/l, r began decreasing slowly while I_1/I_3 continued the increasing trend until the foot of peak-r. From the linearly changing trend of both r and I_1/I_3, it seemed that system was in a slow equilibrating process. This is also reflected on the downwards excursion of system T_m on DSC curves (Fig. 2) and the slow decreasing representative size of assemblies shown by DLS data (Fig. 4H) for this range. However, on DSC curves of the samples containing 1.4 or 3.0 mmol/l of DTEAB, a phase with high T_m appeared at more than 40 °C in addition to one with low T_m nearby 10 °C (Fig. 2). The high T_m nearby 40 °C may indicate formation of microdomains of different composition in same assemblies or some new assemblies being formed with higher molecule packing density in the mixture [28]. The former may be only a preliminary process of the later [29], but no new structure of assemblies form in that case. For the later case, however, the new assemblies can be observed on TEM picture, if present. Actually, in Fig. 3C, a cluster of transversely-cut profiles of extruding tubule-like structures were observed with the FF-TEM specimen containing 3 mmol/l DTEAB. Within our knowledge, it is the first time that tubule-like structures were observed from a transversally-cut profile in FF-TEM during liposome solubilization process.

Tubules have been observed in various amphiphilic systems [30,31], including lipid and cosurfactant mixture, for example, DMPC/genariol/water [32]. Two main theories are tried to explain the formation of tubules. One suggests that the anisotropy of membrane [33], resulted from the symmetry breaking in molecular packing, can lead to tubular structures. Another is chirality in the microstructures [34]. Here, symmetry breaking may be the reason for the appearance of tubules in the DMPC

vesicles solubilization course by DTEAB. The formerly vesicles fission products were not a stable state due to, for example, the asymmetric distribution of membrane composition or phase separation. So addition of little DTEAB may further increase the anisotropy of these new assemblies and lead to their fusion to form tubules finally, which expressed a big peak centered at 82.92 nm in Fig. 4C. In this process, the mixed micelles were also present probably in the system although they could not be detected by the techniques used in this work. The decreasing tendency of system $\langle R_h \rangle$ in Fig. 4H might reflect a slow assembly transformation course, e.g., from lamellar vesicles/tubules to micelles.

4.4. Tubules fission to vesicles

On right half of r curve in Fig. 1, r displayed a peak centering at 8 mmol/l DTEAB. Similar r curve of DPH was observed during vesicle solubilization by sodium cholate in Schubert et al.'s work [4], where the Egg PC/Chol vesicles solubilization process was referred to beginning from the front foot of r peak based on a leakage inspection of entrapped chromophore, and the maximal value of r was considered indicating the completion of vesicle solubilization in that inspected process. In the present work, only small vesicles were observed at the r peak top composition. This indicates that assembly morphology changes occurred before this r peak top. In DLS results of Fig. 4H, $\langle R_h \rangle$ of this sample was 34.58 nm, which indicates the main assemblies in the system were still extraordinarily larger than micelles. On DSC inspection about the same sample (Fig. 2), both primary phases with high or low T_m, on before curves (of samples containing 1.4 and 3 mmol/l of DTEAB) disappeared and were replaced by two phases with overlapped endothermic peaks at 20.3 and 25.5 °C, respectively. Apparently, a large amount of micelles had been produced then since R_h distribution of this sample showed a cluster of assemblies around 3.0 nm in addition to a big one at 36.44 nm in Fig. 4F. Therefore, it can be concluded that at the top of r peak (Fig. 1) those primarily-formed tubule-like assemblies had transformed into vesicles again. In this process, micelles were also produced, which were invisible in the present FF-TEM picture except DLS examination (Fig. 4F). Additionally, the deflection to steep increasing tendency of I_1/I_3 (Fig. 1) is another evidence for the occurrence of assembly morphology transformation as well as the onset of lamellar structure solubilization. The above results agreed well with Schubert et al.'s conclusion [4]. However, it was not purely a vesicle solubilization process in the present work, but a tubule fission process because tubule structure predominated in the system prior to r peak and the final main assemblies at r peak top (Fig. 1) were vesicles (Fig. 3d). The fission of lipid tubules into vesicles from lysophosphatidylcholine had been observed with light microscope in the work of Tanaka et al. [26]. In Fuhrhop's work, a splitting of DMPC tubules into vesicles by addition of dextran with a few hydrophobic side chains was also shown by a light micrograph [30]. All these phenomena suggested that the ability to induce fission of large lamellar assemblies is a general property of detergent molecules.

4.5. Micellization

On the rear half of r peak, further addition of DTEAB caused the collapse of the cluster of large assemblies to micelles while both r and I_1/I_3 changed steeply until the value for pure DTEAB system (20 mmol/l) (Fig. 1) as done in cases of other surfactant [2–4,7,8,21]. Powerful evidence can be obtained from R_h distribution data. In Fig. 4H, $\langle R_h \rangle$ decreased sharply from 34.6 to 8.1 nm even the concentration of DTEAB only increased by 2 mmol/l. As for R_h distribution measurement for sample containing 10 mmol/l of DTEAB in Fig. 4G, a large cluster of micelles was found centering around 6.26 nm even a small peak still present at 55.61 nm, which represent a small amount of survival large assemblies near the end of solubilization process considering the 6th power of R_h dependence of the scattered light intensity. Nevertheless, the present vesicle solubilization process ended with micelles, the natural form of pure DTEAB assemblies in aqueous system. This agreed well with the last stage description of three-stage model [2,3].

5. Conclusion

In the present work, the assembly morphology during the solubilization of DMPC vesicles by DTEAB was investigated with various techniques. A primary model was sketched out to account for assemblies transformation during this process. This model differs with the classical three-stage model mainly on its middle stages, including vesicles division, tubule-like structure formation and fission to vesicles again etc. Especially, the finding of tubule-like structure in the present inspected process was a supplement for the existing theoretical mechanism about assembly transformation during vesicle solubilization.

In this work, the distinct character of DTEAB molecules is its positively charged head group, which brought the static electric repulsion between components into the host assemblies in addition to the hydrophobic affinity effect. Because all the components in the assemblies will be ruled into a relative fixed distribution at equilibrium, distribution of the newcomer in the mixed assemblies is a central problem concerning the most morphology transformation of assemblies before the beginning of vesicle solubilization into micelles. Tracing the changes of their distribution is a pivotal work to give a more clear illustration about mechanism controlling the morphology transformation course during the studied process. Additionally, a try to understand the permeability changes of these various assemblies during the process is also a supplement for the application of this work as done by Lafleur and co-workers [35].

Supplementary material

The online version of this article contains additional supplementary material. Please visit DOI:10.1016/j.jcis.2007.02.053.

References

[1] A. Hlenius, K. Simons, Biochim. Biophys. Acta 415 (1975) 29–79.
[2] K. Edwards, M. Almgren, Langmuir 8 (1992) 824–832.

[3] D. Lichtenberg, R.J. Robson, E.A. Dennis, Biochim. Biophys. Acta 737 (1983) 285–304;
D. Lichtenberg, Biochim. Biophys. Acta 821 (1985) 470–478.

[4] R. Schubert, K. Beyer, H. Wolburg, K.H. Schmidt, Biochemistry 25 (1986) 5263–5269;
R. Schubert, K.H. Schmidt, Biochemistry 27 (1988) 8787–8794.

[5] M. Almgren, Biochim. Biophys. Acta 1508 (2000) 146–163.

[6] T. Inoue, J. Colloid Interface Sci. 149 (1992) 345–358.

[7] (a) K. Edwards, M. Almgren, J. Bellare, W. Brown, Langmuir 5 (1989) 473–478;
(b) K. Edwards, J. Gustafsson, M. Almgren, G. Karlsson, J. Colloid Interface Sci. 161 (1993) 299–309.

[8] (a) P. Vinson, Y. Talmon, A. Walter, Biophys. J. 56 (1989) 669–681;
(b) M. Silvander, G. Karlsson, K. Edwards, J. Colloid Interface Sci. 179 (1996) 104–113.

[9] (a) F. Jahnig, Proc. Natl. Acad. Sci. USA 76 (1979) 6361–6365;
(b) J. Repakova, J.M. Holopainen, M.R. Morrow, M.C. McDonald, I. Capkova, P. Vattulainen, Biophys. J. 88 (2005) 3398–3410;
(c) A. Nakajima, Bull. Chem. Soc. Jpn. 44 (1971) 3272–3277.

[10] (a) K. Kalyanasundaram, J.K. Thomas, J. Am. Chem. Soc. 99 (1977) 2039–2044;
(b) P. Somerharju, Chem. Phys. Lipids 116 (2002) 57–74.

[11] M. Shinitzky, Y. Barenholz, J. Biol. Chem. 249 (1974) 2652–2657.

[12] (a) B.R. Lentz, Y. Barenholz, T.E. Thompson, Biochemistry 15 (1976) 4521–4528;
(b) B.R. Lentz, Y. Barenholz, T.E. Thompson, Biochemistry 15 (1976) 4529–4537.

[13] G. Pistolis, A. Malliaris, Langmuir 13 (1997) 1457–1462.

[14] P.R. Majhi, A. Blume, J. Phys. Chem. B 106 (2002) 10753–10763.

[15] S.J. Ryhanen, J.M.I. Alakoskela, P.K.J. Kinnunen, Langmuir 21 (2005) 5707–5715.

[16] T. Inoue, H. Kawamura, S. Okukado, R. Shimozawa, J. Colloid Interface Sci. 168 (1994) 94–102.

[17] P.R. Majhi, A. Blume, Langmuir 17 (2001) 3844–3851.

[18] J. Martins, E. Melo, Biophys. J. 80 (2001) 832–840.

[19] A. Hildebrand, R. Neubert, P. Garidel, A. Blume, Langmuir 18 (2002) 2836–2847.

[20] T. Inoue, R. Motoyama, M. Totoki, K. Miyakawa, R. Shimozawa, J. Colloid Interface Sci. 164 (1994) 318–324.

[21] (a) O. López, M. Cócera, R. Pons, N. Azemar, C. López-Iglesias, E. Wehrli, J.L. Parra, A. de la Maza, Langmuir 15 (1999) 4678–4681;
(b) M. Ueno, Biochemistry 28 (1989) 5631–5634;

(c) S. Almog, Biochemistry 25 (1986) 2597–2605;
(d) P. Schurtenberger, N. Mazer, W. Kanzig, J. Phys. Chem. 89 (1985) 1042–1049;
(e) K. Edwards, M. Almgren, J. Colloid Interface Sci. 147 (1991) 1–21;
(f) A. Walter, G. Kuehl, K. Barnes, G. VanderWaerdt, Biochim. Biophys. Acta 1508 (2000) 20–33.

[22] M. Ollivon, O. Eidelman, R. Blumenthal, A. Walter, Biochemistry 27 (1988) 1695–1703.

[23] (a) R.E. Davenport, L. Dale, R.H. Bisby, R.B. Cundall, Biochemistry 24 (1985) 4097–4108;
(b) S.Y. Chen, K.H. Cheng, Biophys. J. 71 (1996) 878–884.

[24] (a) M.P. Sheetz, S.J. Singer, Proc. Natl. Acad. Sci. USA 71 (1974) 4457–4461;
(b) A. Iglic, H. Hagerstrand, Med. Biol. Eng. Comput. 37 (1999) 125–129.

[25] G. Staneva, M. Seigneuret, K. Koumanov, G. Trugnan, M.I. Angelova, Chem. Phys. Lipids 136 (2005) 55–66.

[26] T. Tanaka, R. Sano, Y. Yamashita, M. Yamazaki, Langmuir 20 (2004) 9526–9534.

[27] T. Baumgart, S.T. Hess, W.W. Webb, Nature 425 (2003) 821–824.

[28] (a) P.C.A. Barreleiro, G. Olofsson, W. Brown, K. Edwards, N.M. Bonassi, E. Feitosa, Langmuir 18 (2002) 1024–1029;
(b) G. Cevc, H. Richardsen, Adv. Drug Delivery Rev. 38 (1999) 207–232.

[29] A. Roux, D. Cuvelier, P. Nassoy, J. Prost, P. Bassereau, B. Goud, EMBO J. 24 (2005) 1537–1545.

[30] J.H. Fuhrhop, Chem. Rev. 93 (1993) 1582–1585.

[31] (a) J.M. Schnur, Science 262 (1993) 1669–1676;
(b) G.W. Orr, L.J. Barbour, J.L. Atwood, Science 285 (1999) 1049–1052.

[32] S. Chiruvolu, H.E. Warriner, E. Naranjo, S.H.J. Idziak, J.O. Rädler, R.J. Plano, J.A. Zasadzinski, C.R. Safinya, Science 266 (1994) 1222–1225.

[33] (a) T.C. Lubensky, J. Prost, J. Phys. II 2 (1992) 371–382;
(b) C.M. Chen, Phys. Rev. E 59 (1999) 6192–6195;
(c) H. Von Berlepsch, C. Böttcher, A. Ouart, M. Regenbrecht, S. Akari, U. Keiderling, H. Schnablegger, S. Dähne, S. Kirstein, Langmuir 16 (2000) 5908–5916.

[34] (a) W. Helfrich, J. Prost, Phys. Rev. A 38 (1988) 3065–3068;
(b) M.S. Spector, R.R. Price, J.M. Schnur, Adv. Mater. 11 (1999) 337–340;
(c) S.B. Lee, R. Koepsel, D.B. Stolz, H. Warriner, A.J. Russell, J. Am. Chem. Soc. 126 (2004) 13400–13405.

[35] L. Marcotte, J. Barbeau, M. Lafleur, J. Colloid Interface Sci. 292 (2005) 219–227.